

MODULAR NONLINEAR FILTER BASED TIME RELAXATION SCHEME FOR HIGH REYNOLDS NUMBER FLOWS

AZIZ TAKHIROV, MONIKA NEDA, AND JIAJIA WATERS

(Communicated by L. Rebholz)

This paper is dedicated to Professor William Layton's 60th birthday.

Abstract. In this article, we propose and develop a time relaxation implementation of the modular nonlinear filter model of [21]. A complete numerical analysis of the scheme, that includes the computability of its numerical solutions, its stability, and velocity error estimates, is given. This is followed by 2D and 3D numerical experiments that show the advantage of the proposed scheme.

Key words. Time relaxation, finite element, nonlinear filtering, deconvolution, Navier-Stokes equations

1. Introduction

The range of size of the velocity eddies is very wide, especially in simulation with higher Reynolds number. Based on the Kolmogorov theory [16], the computations have to be done on a very fine mesh to be able to capture all the persistent eddies and these proper numerical computations are not feasible with the current computer power. For this reason, numerical regularization and computational stabilizations have been explored in computational fluid dynamics, [4, 26, 15]. Herein, we study a regularization that has been proposed by Adams, Stoltz and Kleiser [1, 2, 29, 30]. Let \mathbf{u} represent the fluid velocity, h the characteristic mesh width, and $\delta = O(h)$ a chosen length scale, and \mathbf{u}' denote some representation of the part of \mathbf{u} varying over length scales $< O(\delta)$, i.e., the fluctuating part of \mathbf{u} . This will be made specific in Section 2 and 3. The fluid regularization model that we consider, was obtained by adding a time regularization term, $\chi\mathbf{u}'$ to the Navier-Stokes equations (NSE)

$$(1) \quad \mathbf{u}_t + \mathbf{u} \cdot \nabla \mathbf{u} + \nabla p - \nu \Delta \mathbf{u} + \chi \mathbf{u}' = \mathbf{f}, \quad x \in \Omega,$$

$$(2) \quad \nabla \cdot \mathbf{u} = 0, \quad x \in \Omega.$$

The term $\chi\mathbf{u}'$ is a linear, lower order term and it is intended to drive unresolved velocity scales to zero exponentially fast. With that aim, $\chi > 0$, and has units of $1/time$. The regularizations of this type have been extensively studied in the literatures. Adams, Kleiser and Stoltz have performed numerical tests of this time relaxation model on compressible flows with shocks and on turbulent flows, [28, 29, 30]. Guenanff [11] performed studies on aerodynamic noise. Rosenau [25], Schochet and Tadmor [27] did studies of (1)-(2) in which the time relaxation model was developed from a regularized Chapman-Enskog expansion of conservation laws. In [22], it was shown that at high Reynolds number, solutions to (1)-(2), possess an energy cascade which terminates at the mesh scale δ with the proper choice of relaxation coefficient χ . Also, the joint helicity/energy cascade was investigated in [20]. A standard continuous finite element analysis of the model (1)-(2) was performed in [10].

In [24], following the work from [6], it was also studied a continuous finite element discretization of (1)-(2) that incorporated three ideas. First idea was to use incompressible filter (i.e. a Stokes type of filter problem) for better consistency outside of the periodic domains. Second idea was the efficient implementation of linearization of Baker [3], that allows to solve for only one linear system per time step with second order of accuracy. The third idea was the stabilization in time that is natural for this linearization and which was first introduced in [17].

The goal of this paper is to present the implementation of the time-relaxation regularization through the nonlinear filter stabilization method of [21]. The attractive feature of the modular adaptive nonlinear filter model [21] is that it allows one to incorporate a desired eddy-viscosity model into the legacy codes by solving an additional Stokes-Darcy type system, as mentioned in [5]. The idea has been further extended to improve the Leray- α model in [7], and a first order, computationally efficient implementation has been recently reported in [9]. The proposed scheme is also easy to incorporate into the existing codes. It requires solution of the Stokes like system (or just an elliptic problem, since Laplace type of filtering showed comparable results to Stokes for the few performed numerical experiments), and changing the coefficient in the mass matrix.

This article is organized the following way. In Section 2 we give a precise definition of the discrete nonlinear filtering operator and of the generalized fluctuation \mathbf{u}' . We also give preliminaries about the finite element framework. Section 3 gives the scheme and its unconditionally stability. In Section 4 the finite element convergence error analysis is presented. In Section 5, we present 2D and 3D numerical tests that show the effectiveness of the nonlinear filters for the time relaxation model.

2. Notation and Preliminaries

In order to discuss the effects of the regularization we introduce the following notation. The $L^2(\Omega)$ norm and inner product will be denoted by $\|\cdot\|$ and (\cdot, \cdot) . Likewise, the $L^p(\Omega)$ norms and the Sobolev $W_p^k(\Omega)$ norms are denoted by $\|\cdot\|_{L^p}$ and $\|\cdot\|_{W_p^k}$, respectively. For the semi-norm in $W_p^k(\Omega)$ we use $|\cdot|_{W_p^k}$. H^k is used to represent the Sobolev space W_2^k , and $\|\cdot\|_k$ denotes the norm in H^k . For functions $\mathbf{v}(\mathbf{x}, t)$ defined on the entire time interval $(0, T)$, we define

$$\|\mathbf{v}\|_{\infty, k} := \sup_{0 < t < T} \|\mathbf{v}(\cdot, t)\|_k, \quad \text{and} \quad \|\mathbf{v}\|_{m, k} := \left(\int_0^T \|\mathbf{v}(\cdot, t)\|_k^m dt \right)^{1/m}.$$

The following function spaces are used in the analysis:

$$\begin{aligned} \text{Velocity Space} & - X := H_0^1(\Omega), \\ \text{Pressure Space} & - P := L_0^2(\Omega) = \left\{ q \in L^2(\Omega) : \int_{\Omega} q d\Omega = 0 \right\}, \\ \text{Divergence - free Space} & - Z := \left\{ \mathbf{v} \in X : \int_{\Omega} q \nabla \cdot \mathbf{v} d\Omega = 0, \forall q \in P \right\}. \end{aligned}$$

We denote the dual space of X as X' , with norm $\|\cdot\|_{-1}$.

Let $\Omega \subset \mathbb{R}^d$ ($d = 2, 3$) be a polygonal domain and let T_h be a triangulation of Ω made of triangles (in \mathbb{R}^2) or tetrahedrons (in \mathbb{R}^3). Thus, the computational domain is defined by

$$\Omega = \cup K; \quad K \in T_h.$$

We assume that there exist constants c_1, c_2 such that

$$c_1 h \leq h_K \leq c_2 \rho_K$$

where h_K is the diameter of triangle (tetrahedral) K , ρ_K is the diameter of the greatest ball (sphere) included in K , and $h = \max_{K \in T_h} h_K$. Let $P_k(K)$ denote the space of polynomials on K of degree no greater than k . Then we define the finite element spaces as follows.

$$\begin{aligned} X_h &:= \{ \mathbf{v} \in X \cap C(\bar{\Omega}) : \mathbf{v}|_K \in P_k(K), \forall K \in T_h \}, \\ P_h &:= \{ q \in P \cap C(\bar{\Omega}) : q|_K \in P_s(K), \forall K \in T_h \}, \\ Z_h &:= \{ \mathbf{v} \in X_h : (q, \nabla \cdot \mathbf{v}) = 0, \forall q \in P_h \}. \end{aligned}$$

We assume that the spaces X_h, P_h satisfy the discrete inf-sup condition [12], namely there exists $\gamma \in \mathbb{R}, \gamma > 0$,

$$(3) \quad \gamma \leq \inf_{q_h \in P_h} \sup_{\mathbf{v}_h \in X_h} \frac{(q_h, \nabla \cdot \mathbf{v}_h)}{\|q_h\| \|\nabla \mathbf{v}_h\|}.$$

Taylor-Hood elements are an example of such a space with $k = 2$ and $s = 1$, [8, 12, 18].

Let Δt be the step size for t so that $t_n = n\Delta t, n = 0, 1, 2, \dots, N_T$, with $T := N_T \Delta t$, and $d_t f^n := \frac{f(t_n) - f(t_{n-1})}{\Delta t}$. We define the following additional norms:

$$\|\mathbf{v}\|_{\infty, k} := \max_{0 \leq n \leq N_T} \|\mathbf{v}^n\|_k, \quad \|\mathbf{v}\|_{m, k} := \left(\sum_{n=0}^{N_T} \|\mathbf{v}^n\|_k^m \Delta t \right)^{1/m}.$$

Also, we make use of the following approximation properties, [8]:

$$(4) \quad \begin{aligned} \inf_{\mathbf{v} \in X_h} \|\mathbf{u} - \mathbf{v}\| &\leq Ch^{k+1} \|\mathbf{u}\|_{k+1}, \quad \mathbf{u} \in H^{k+1}(\Omega)^d, \\ \inf_{\mathbf{v} \in X_h} \|\mathbf{u} - \mathbf{v}\|_1 &\leq Ch^k \|\mathbf{u}\|_{k+1}, \quad \mathbf{u} \in H^{k+1}(\Omega)^d, \\ \inf_{r \in P_h} \|p - r\| &\leq Ch^{s+1} \|p\|_{s+1}, \quad p \in H^{s+1}(\Omega). \end{aligned}$$

We define the *skew-symmetric trilinear form* $b^*(\cdot, \cdot, \cdot) : X \times X \times X \rightarrow \mathbb{R}$ as in [18]

$$(5) \quad b^*(\mathbf{u}, \mathbf{v}, \mathbf{w}) := \frac{1}{2}(\mathbf{u} \cdot \nabla \mathbf{v}, \mathbf{w}) - \frac{1}{2}(\mathbf{u} \cdot \nabla \mathbf{w}, \mathbf{v}).$$

Note that for $\mathbf{u}, \mathbf{v}, \mathbf{w}, \in X$, with $\mathbf{u} \in Z$,

$$b^*(\mathbf{u}, \mathbf{v}, \mathbf{w}) = (\mathbf{u} \cdot \nabla \mathbf{v}, \mathbf{w}).$$

The error analysis uses the discrete Gronwall inequality.

Lemma 2.1 (Discrete Gronwall Lemma). *Let $\Delta t, H$, and a_n, b_n, c_n, d_n (for integers $n \geq 0$) be finite nonnegative numbers such that*

$$(6) \quad a_l + \Delta t \sum_{n=0}^l b_n \leq \Delta t \sum_{n=0}^{l-1} d_n a_n + \Delta t \sum_{n=0}^l c_n + H \quad \text{for } l \geq 1.$$

Then for $\Delta t > 0$

$$(7) \quad a_l + \Delta t \sum_{n=0}^l b_n \leq \exp \left(\Delta t \sum_{n=0}^{l-1} d_n \right) \left(\Delta t \sum_{n=0}^l c_n + H \right) \quad \text{for } l \geq 1.$$

Definition 2.1. Define the L^2 projection, $P_{Z_h} : L^2(\Omega) \rightarrow Z_h$, by

$$(P_{Z_h}(\mathbf{v}) - \mathbf{v}, \mathbf{w}) = 0, \quad \forall \mathbf{w} \in Z_h.$$

2.1. Nonlinear Filtering. The filter we consider herein was first proposed in [21]. It is based on the physical idea that in laminar regions, or in the regions where coherent structures persist, little or no filtering is needed because these regions are resolvable. This idea is implemented through the nonlinear filter

$$-\alpha^2 \nabla \cdot (a(\mathbf{u}) \nabla \bar{\mathbf{u}}) + \bar{\mathbf{u}} = \mathbf{u},$$

where $a(\mathbf{u})$ satisfies:

- $0 \leq a(\mathbf{u}) \leq 1$ for any fluid velocity $\mathbf{u}(\mathbf{x}, t)$,
- $a(\mathbf{u}) \simeq 0$ selects regions requiring no local filtering,
- $a(\mathbf{u}) \simeq 1$ selects regions requiring $O(\alpha)$ local filtering.

The function $a(\mathbf{u})$ is called an indicator function, and it allows to vary the filtering radius between 0 and 1, depending on the local flow structures. In the discrete setting, $\alpha = \mathcal{O}(h)$. Herein, we study the following possible choices of indicator functions.

The Q criterion-based indicator: The Q criterion, developed in [32], is one the most popular method for eduction of coherent vortices. First, we define deformation and spin tensors respectively by

$$\nabla^s \mathbf{u} := \frac{1}{2}(\nabla \mathbf{u} + \nabla \mathbf{u}^T) \text{ and } \nabla^{ss} \mathbf{u} := \frac{1}{2}(\nabla \mathbf{u} - \nabla \mathbf{u}^T).$$

A persistent and coherent vortex is found in regions where spin dominates deformation, i.e., where the following is satisfied,

$$Q(\mathbf{u}, \mathbf{u}) := \frac{1}{2}(\nabla^{ss} \mathbf{u} : \nabla^{ss} \mathbf{u} - \nabla^s \mathbf{u} : \nabla^s \mathbf{u}) > 0.$$

We define our Q criterion-based indicator function such that $Q(\mathbf{u}, \mathbf{u}) > 0$ implies $a(\mathbf{u}) \simeq 0$. One of the ways to implement this is by defining

$$a_Q(\mathbf{u}) := \frac{1}{2} - \frac{1}{\pi} \arctan \left(\alpha^{-1} \frac{Q(\mathbf{u}, \mathbf{u})}{|Q(\mathbf{u}, \mathbf{u})| + \alpha^2} \right).$$

Vreman's eddy viscosity-based indicator: Vreman constructed an eddy viscosity coefficient formula that vanishes identically for 320 types of flow structures that are known to be coherent (non turbulent). This is presented in [31], and it is achieved using only the gradient tensor. First, we define

$$\begin{aligned} |\nabla \mathbf{u}|_F^2 &= \sum_{i,j=1,2,3} \left(\frac{\partial u_j}{\partial x_i} \right)^2, \\ \beta_{i,j} &:= \sum_{m=1,2,3} \frac{\partial u_i}{\partial x_m} \frac{\partial u_j}{\partial x_m}, \text{ and} \\ B(\mathbf{u}) &:= \beta_{11}\beta_{22} - \beta_{12}^2 + \beta_{11}\beta_{33} - \beta_{13}^2 + \beta_{22}\beta_{33} - \beta_{23}^2. \end{aligned}$$

Then, Vreman's eddy viscosity coefficient equals to

$$\nu_T = C\alpha^2 \sqrt{\frac{B(\mathbf{u})}{|\nabla \mathbf{u}|_F^4}} \text{ if } |\nabla \mathbf{u}|_F \neq 0 \text{ or } 0, \text{ otherwise,}$$

where C is a positive constant. Using that $0 \leq \frac{B(\mathbf{u})}{|\nabla \mathbf{u}|_F^4} \leq 1$, we define

$$a_V(\mathbf{u}) := \sqrt{\frac{B(\mathbf{u})}{|\nabla \mathbf{u}|_F^4}}.$$

Synthesized methods: The advantage of this method is that combines two indicator functions that have different selection criteria. Thus, given indicator functions a_i , we construct synthesized indicator functions as

$$a_{ij}(\mathbf{u}) := (a_i(\mathbf{u})a_j(\mathbf{u}))^{1/2}.$$

More details on the above indicator functions can be found in [21].

2.1.1. Discrete filtering. Given an indicator function $a(\cdot)$, a fluid velocity \mathbf{u} , an averaging radius α , we define the filtered velocity $\bar{\mathbf{u}}^h$ using a selected indicator function, $a(\cdot)$, as the solution of: Find $(\bar{\mathbf{u}}^h, \lambda_h) \in X_h \times P_h$ satisfying

$$(8) \quad \alpha^2(a(\mathbf{u})\nabla \bar{\mathbf{u}}^h, \nabla \mathbf{v}_h) + (\bar{\mathbf{u}}^h, \mathbf{v}_h) = (\mathbf{u}, \mathbf{v}_h), \quad \forall \mathbf{v}_h \in X_h,$$

To impose divergence free of the filtered velocity, we considered Stokes type non-linear filter defined as: Find $(\bar{\mathbf{u}}^h, \lambda_h) \in X_h \times P_h$ satisfying

$$(9) \quad \alpha^2(a(\mathbf{u})\nabla \bar{\mathbf{u}}^h, \nabla \mathbf{v}_h) + (\bar{\mathbf{u}}^h, \mathbf{v}_h) - (\lambda_h, \nabla \cdot \mathbf{v}_h) = (\mathbf{u}, \mathbf{v}_h), \quad \forall \mathbf{v}_h \in X_h,$$

$$(10) \quad (\nabla \cdot \bar{\mathbf{u}}^h, q) = 0, \quad \forall q \in P_h.$$

Given $\mathbf{u} \in X$, the nonlinear filtering step is a linear problem. It is straightforward to show the well-posedness of (8), and (9)-(10). In particular, the solution satisfies

$$2 \int_{\Omega} \alpha^2 a(\mathbf{u}) |\nabla \bar{\mathbf{u}}^h|^2 dx + \|\bar{\mathbf{u}}^h\|^2 \leq \|\mathbf{u}\|^2,$$

stability estimate and following error estimate.

Theorem 2.1. *Let $\bar{\mathbf{u}}^h$ be the solution of (9)-(10), and $\mathbf{u} \in Z_h$. Then*

$$\begin{aligned} & \int_{\Omega} \alpha^2 a(\mathbf{u}) |\nabla(\mathbf{u} - \bar{\mathbf{u}}^h)|^2 dx + \|\mathbf{u} - \bar{\mathbf{u}}^h\|^2 \\ & \leq C \inf_{\tilde{\mathbf{u}} \in X_h} (\int_{\Omega} \alpha^2 a(\mathbf{u}) |\nabla(\mathbf{u} - \tilde{\mathbf{u}})|^2 dx + \|\mathbf{u} - \tilde{\mathbf{u}}\|^2) + C\alpha^4 \|\nabla \cdot (a(\mathbf{u})\nabla \mathbf{u})\|^2. \end{aligned}$$

The proofs are given in [7].

3. Time Relaxation Scheme and Stability

This section introduces the scheme studied herein in Algorithm 3.1 and proves unconditional stability. The chosen time discretization is based on linearly extrapolated backward Euler scheme. The time relaxed, discrete approximation to (1)-(2) on the time interval $(0, T]$, is given by the following algorithm.

Algorithm 3.1. *Let $\mathbf{u}_h^0 := P_{Z_h}(\mathbf{u}_0)$.*

For $n = 0, 1, 2, \dots, M-1$, where $M := \frac{T}{\Delta t}$, find $\mathbf{u}_h^{n+1} \in X_h$, $p_h^{n+1} \in P_h$, such that

$$(11) \quad \frac{1}{\Delta t} (\mathbf{u}_h^{n+1} - \mathbf{u}_h^n, \mathbf{v}_h) + b^*(\mathbf{u}_h^n, \mathbf{u}_h^{n+1}, \mathbf{v}_h) + \nu (\nabla \mathbf{u}_h^{n+1}, \nabla \mathbf{v}_h) - (p_h^{n+1}, \nabla \cdot \mathbf{v}_h) + \chi (\mathbf{u}_h^{n+1} - \bar{\mathbf{u}}_h^n, \mathbf{v}_h) = (\mathbf{f}(t^{n+1}), \mathbf{v}_h), \quad \forall \mathbf{v}_h \in X_h,$$

$$(12) \quad (\nabla \cdot \mathbf{u}_h^{n+1}, q_h) = 0, \quad \forall q_h \in P_h.$$

Lemma 3.1. *The scheme (11)-(12) has a unique solution and satisfies*

$$\|\mathbf{u}_h^M\|^2 + \chi \Delta t \|\mathbf{u}_h^{M-1}\|^2 + \nu \Delta t \sum_{n=0}^{M-1} \|\nabla \mathbf{u}_h^{n+1}\|^2 \leq C(\mathbf{f}, \mathbf{u}_0, \chi, \nu).$$

Proof: Let $\mathbf{v}_h = \mathbf{u}_h^{n+1}$ in (11), $q_h = p_h^{n+1}$ in (12), and add the equations to get

$$\begin{aligned} \frac{1}{\Delta t} (\mathbf{u}_h^{n+1} - \mathbf{u}_h^n, \mathbf{u}_h^{n+1}) + \nu (\nabla \mathbf{u}_h^{n+1}, \nabla \mathbf{u}_h^{n+1}) + \chi (\mathbf{u}_h^{n+1} - \overline{\mathbf{u}}_h^{n+1}, \mathbf{u}_h^{n+1}) \\ = (\mathbf{f}(t^{n+1}), \mathbf{u}_h^{n+1}). \end{aligned}$$

Standard inequalities give

$$\begin{aligned} \frac{1}{2\Delta t} (\|\mathbf{u}_h^{n+1}\|^2 - \|\mathbf{u}_h^n\|^2) + \nu \|\nabla \mathbf{u}_h^{n+1}\|^2 + \chi \|\mathbf{u}_h^{n+1}\|^2 \\ = \chi (\overline{\mathbf{u}}_h^{n+1}, \mathbf{u}_h^{n+1}) + (\mathbf{f}(t^{n+1}), \mathbf{u}_h^{n+1}) \\ \leq \frac{\nu}{2} \|\nabla \mathbf{u}_h^{n+1}\|^2 + \frac{1}{2\nu} \|\mathbf{f}(t^{n+1})\|_{-1}^2 + \frac{\chi}{2} \|\overline{\mathbf{u}}_h^{n+1}\|^2 + \frac{\chi}{2} \|\mathbf{u}_h^{n+1}\|^2, \\ \leq \frac{\nu}{2} \|\nabla \mathbf{u}_h^{n+1}\|^2 + \frac{1}{2\nu} \|\mathbf{f}(t^{n+1})\|_{-1}^2 + \frac{\chi}{2} \|\mathbf{u}_h^n\|^2 + \frac{\chi}{2} \|\mathbf{u}_h^{n+1}\|^2, \end{aligned}$$

i.e.,

$$(13) \quad \frac{1}{2\Delta t} (\|\mathbf{u}_h^{n+1}\|^2 - \|\mathbf{u}_h^n\|^2) + \frac{\chi}{2} (\|\mathbf{u}_h^{n+1}\|^2 - \|\mathbf{u}_h^n\|^2) + \frac{\nu}{2} \|\nabla \mathbf{u}_h^{n+1}\|^2 \leq \frac{1}{2\nu} \|\mathbf{f}(t^{n+1})\|_{-1}^2,$$

Summing over the time steps $n = 0 \dots M-1$ gives

$$(14) \quad \frac{1}{2\Delta t} (\|\mathbf{u}_h^M\|^2 - \|\mathbf{u}_h^0\|^2) + \frac{\chi}{2} (\|\mathbf{u}_h^M\|^2 - \|\mathbf{u}_h^0\|^2) + \frac{\nu}{2} \sum_{n=0}^{M-1} \|\nabla \mathbf{u}_h^{n+1}\|^2 \leq \frac{1}{2\nu} \sum_{n=0}^{M-1} \|\mathbf{f}(t^{n+1})\|_{-1}^2.$$

Multiplying by $2\Delta t$, yields

$$(15) \quad (1 + \chi\Delta t) \|\mathbf{u}_h^M\|^2 + \nu\Delta t \sum_{n=0}^{M-1} \|\nabla \mathbf{u}_h^{n+1}\|^2 \leq \nu^{-1}\Delta t \sum_{n=0}^{M-1} \|\mathbf{f}(t^{n+1})\|_{-1}^2 + (1 + \chi\Delta t) \|\mathbf{u}_h^0\|^2.$$

Since the scheme is finite dimensional and linear, the existence of the solution is equivalent to its uniqueness. From (15) it follows that if $\mathbf{u}_h^0 = \mathbf{f} = \mathbf{0}$, then $\mathbf{u}_h^n = \mathbf{0}$ and therefore, $p_h^n = 0$ due to the inf-sup condition.

4. Finite Element Error Analysis

We study the error between the finite element solution of the scheme and solution of Navier-Stokes equations. We introduce a variational solution of the NSE as: *Find* $(\mathbf{u}(x, t), p(x, t))$ *satisfying*

$$(16) \quad (\mathbf{u}_t, \mathbf{v}) + (\mathbf{u} \cdot \nabla \mathbf{u}, \mathbf{v}) - (p, \nabla \cdot \mathbf{v}) + \nu(\nabla \mathbf{u}, \nabla \mathbf{v}) = (\mathbf{f}, \mathbf{v}), \quad \forall \mathbf{v} \in X,$$

$$(17) \quad (q, \nabla \cdot \mathbf{u}) = 0, \quad \forall q \in P,$$

$$(18) \quad \mathbf{u}(\mathbf{x}, 0) = \mathbf{u}_0(\mathbf{x}), \quad \forall \mathbf{x} \in \Omega.$$

Theorem 4.1. *Let $(\mathbf{u}(t), p(t))$ be a sufficiently smooth solution of the NSE satisfying no-slip boundary conditions, with given $\mathbf{f} \in L^\infty(0, T; H^{-1}(\Omega))$ and $\mathbf{u}_0 \in H^1(\Omega)$. Let $(\mathbf{u}_h^n, p_h^n), n = 0, 1, \dots, M$, be the solution of Algorithm 3.1, using*

$(P_k, P_{k-1})(k \geq 2)$ elements. Then, the velocity error $\mathbf{e}^n := \mathbf{u}(x, t_n) - \mathbf{u}_h^n$ satisfies

$$(19) \quad \|\mathbf{e}^N\|^2 + \nu \Delta t \sum_{n=1}^N \|\nabla \mathbf{e}^n\|^2 \leq C(\nu, \mathbf{u}_0, \mathbf{f}, \mathbf{u}, p) (\alpha^2 h^{2k} + h^{2k+2} + \Delta t^2).$$

Proof: Since $\chi = 0$ case is standard, we will only concentrate on the error terms due to the time relaxation term. For the rest of the proof, abusing the notation, we will let $\bar{\mathbf{v}}^h$ be the discrete filter of a generic function $\mathbf{v} \in X$, but with $a(\mathbf{u}_h^n)$ indicator function, instead of $a(\mathbf{v})$. In particular, this means that the filtering operation is linear at each time step. Then the error equation becomes

$$(20) \quad \dots + \chi(\mathbf{e}_{n+1} - \bar{\mathbf{e}}_n, \mathbf{v}_h) = \dots + \chi(\mathbf{u}(t_{n+1}) - \overline{\mathbf{u}(t_n)}, \mathbf{v}_h)$$

Let $\mathbf{U}_h^n \in X_h$ be the interpolant of the exact solution $\mathbf{u}(t_n)$. We decompose the error as $\mathbf{e}_n = (\mathbf{u}(t_n) - \mathbf{U}_h^n) + (\mathbf{U}_h^n - \mathbf{u}_h^n) =: \boldsymbol{\eta}^n + \boldsymbol{\phi}_h^n$, then choose the test function $\mathbf{v}_h = \boldsymbol{\phi}_h^{n+1}$ to get

$$\begin{aligned} & \dots + \frac{\chi}{2} [\|\boldsymbol{\phi}_h^{n+1}\|^2 - \|\boldsymbol{\phi}_h^n\|^2 + \|\boldsymbol{\phi}_h^{n+1} - \boldsymbol{\phi}_h^n\|^2] \\ & \leq \dots - \chi(\boldsymbol{\eta}^{n+1} - \bar{\boldsymbol{\eta}}^n, \boldsymbol{\phi}_h^{n+1}) + \chi(\mathbf{u}(t_{n+1}) - \mathbf{u}(t_n), \boldsymbol{\phi}_h^{n+1}) \\ & \quad + \chi(\mathbf{u}(t_n) - \overline{\mathbf{u}(t_n)}, \boldsymbol{\phi}_h^{n+1}), \end{aligned}$$

where we made use of the fact that $\|\overline{\boldsymbol{\phi}_h^n}\| \leq \|\boldsymbol{\phi}_h^n\|$, as in the stability proof. Now it remains to bound the terms on the right hand side of (21). The standard inequalities yield

$$\begin{aligned} & \chi(\boldsymbol{\eta}^{n+1} - \bar{\boldsymbol{\eta}}^n, \boldsymbol{\phi}_h^{n+1}) \\ & \leq \chi(\|\boldsymbol{\eta}^{n+1} - \boldsymbol{\eta}^n\| + \|\boldsymbol{\eta}^n - \bar{\boldsymbol{\eta}}^n\|) \|\boldsymbol{\phi}_h^{n+1}\| \\ & \leq \varepsilon \nu \|\nabla \boldsymbol{\phi}_h^{n+1}\|^2 + C(\Delta t h^{2k+2} \|\mathbf{u}_t\|_{L^2((t_n, t_{n+1}); H^{k+1}(\Omega))}^2 + \|\boldsymbol{\eta}^n - \bar{\boldsymbol{\eta}}^n\|^2). \end{aligned}$$

The term $\|\boldsymbol{\eta}^n - \bar{\boldsymbol{\eta}}^n\|$ can be bounded using the Proposition 5.4 of [21], giving

$$\|\boldsymbol{\eta}^n - \bar{\boldsymbol{\eta}}^n\| \leq C(h^{2k} \alpha^2 \|\mathbf{u}(t_n)\|_{k+1}^2 + h^{2k+2} \|\mathbf{u}(t_n)\|_{k+1}^2).$$

The remaining two terms are easy to bound. By Taylor series,

$$\begin{aligned} & \chi(\mathbf{u}(t_{n+1}) - \mathbf{u}(t_n), \boldsymbol{\phi}_h^{n+1}) \\ & \leq \varepsilon \nu \|\nabla \boldsymbol{\phi}_h^{n+1}\|^2 + C \Delta t \|\mathbf{u}_t\|_{L^2((t_n, t_{n+1}); L^2(\Omega))}^2 \end{aligned}$$

and using the Proposition 5.4 of [21] one more time, we get

$$\begin{aligned} & \chi(\mathbf{u}(t_n) - \overline{\mathbf{u}(t_n)}, \boldsymbol{\phi}_h^{n+1}) \\ & \leq \varepsilon \nu \|\nabla \boldsymbol{\phi}_h^{n+1}\|^2 + C(h^{2k} \alpha^2 \|\mathbf{u}(t_n)\|_{k+1}^2 + h^{2k+2} \|\mathbf{u}(t_n)\|_{k+1}^2). \end{aligned}$$

Picking ε appropriately, summing over the time steps, Gronwall's and the triangle inequality yields the desired result.

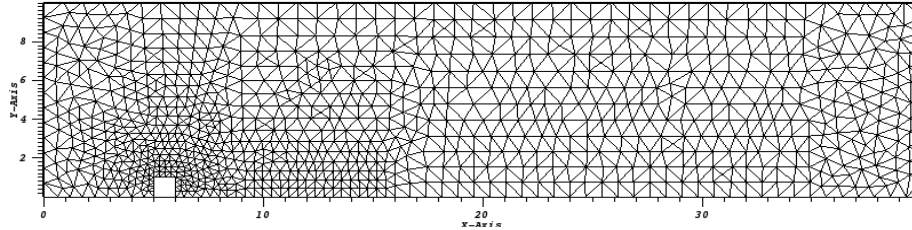


FIGURE 5.1. coarser mesh for the 2D channel flow over a step.

5. Numerical Experiments

In this chapter we present three numerical experiments which illustrate the effectiveness of our scheme defined in the Algorithm 3.1. We use the software FreeFem++ to run the numerical tests, [13]. The Taylor-Hood finite element spaces, i.e., second order polynomial approximations for velocity and first order polynomial approximations for pressure, are used for all simulations.

5.1. 2D channel flow over a step. Our first numerical experiment is for a 2D flow over a forward and backward facing step. We have the same set up as in [7]. The domain is a 40×10 rectangular channel with a 1×1 step five units into the channel at the bottom. We assume no-slip boundary conditions on the top and bottom boundaries, a parabolic infow profile given by $(y(10-y)/25, 0)^T$ and a zero-traction (do-nothing) outflow. The correct behavior is a smooth velocity field away from the step and for eddies to periodically form and shed behind the step. The direct NSE results with different mesh sizes have been presented in [7] and when the mesh size is with 21,593 DOF, the eddy formation and detachment is well captured behind the step. We will test our proposed Algorithm 3.1 with $\chi = 0.1$ combined with Stokes filter on coarser mesh with mesh size $h = 0.937406$ in Figure 5.1 and the time step is $\Delta t = 0.01$, viscosity $\nu = 1/600$ and final time $T = 40$. The filter radius δ is the mesh size. The velocity streamlines over speed contour are shown in Figures 5.2 with different indicator functions $a(u) = 1$, a_V , a_Q and a_{VQ} under the mesh with 4,892 DOF. We can see from the figures that $a(u) = 1$ and Q indicator tend to smooth the solution, not being able to capture more detailed fluid structures. Vreman filter and VQ-filter capture the correct eddy detachment behind the step. The contour plots of different indicator functions at final time $T = 40$ are shown in Figure 5.3. We see that for Vreman and VQ indicator, filters are needed throughout the entire domain. For Q filter, we see near the step, there are filters or no filter, but the rest of the domain has value close to 0.5, which indicates $Q(u, u) = 0$ and additional tuning of a_Q may be needed for this particular problem like [7] suggested. Plots on even coarser mesh ($h = 2.1135$ and 1,762 DOF) Figure 5.4 is presented in Figure 5.5 with VQ indicator and without time relaxation model, and we get a good result with our model and VQ indicator that shows predicted eddy formation and detachment. Without our model, the solution doesn't even converge shown in Figure 5.5 bottom plot.

5.2. 2D Flow around a cylinder. The second numerical experiment is for a 2D flow around a cylinder. This popular benchmark problem has been investigated in [21] and [33]. The patterns are driven by the change of the pressure near the cylinder. The domain of this problem is a 2.2×0.41 rectangular channel with a cylinder of radius 0.05 centered at $(0.2, 0.2)$ (taking the bottom left corner of the

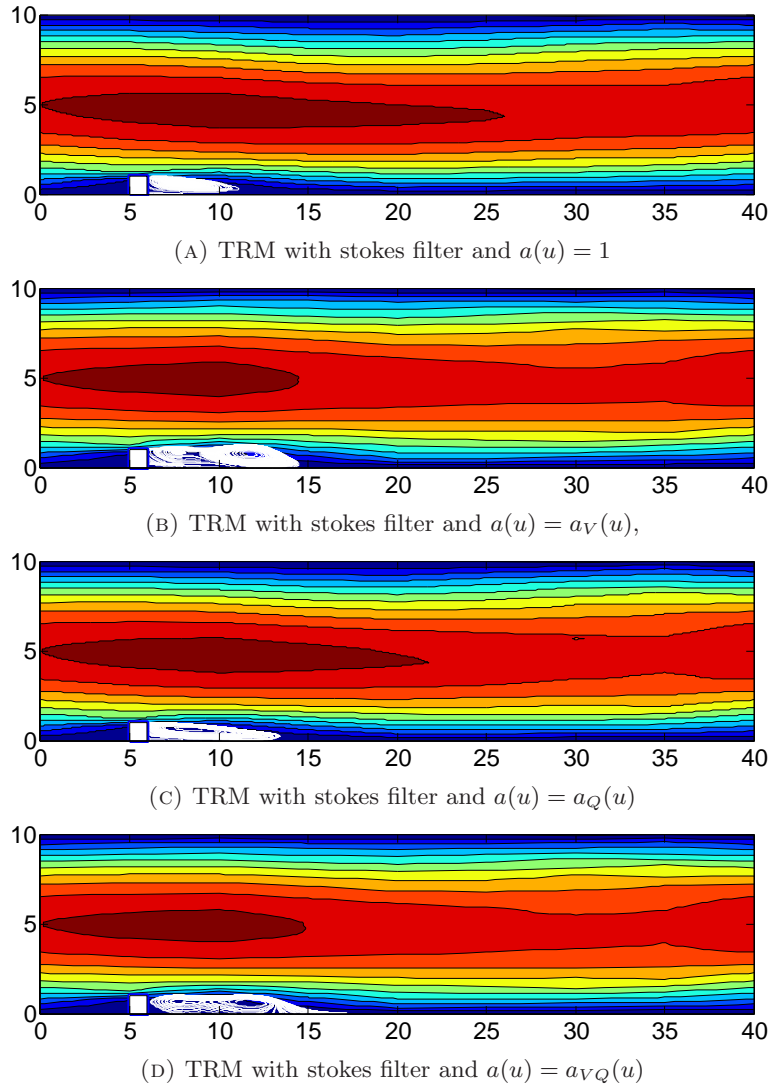


FIGURE 5.2. Velocity solutions for $T = 40$ for 2D flow over a step for the Time Relaxation model with $\chi = 0.1$ using different indicator functions.

rectangle as the origin). The cylinder, top and bottom of the channel are prescribed no-slip boundary conditions, and the time dependent inflow and outflow profiles are

$$\begin{aligned}
 u_1(0, y, t) &= u_1(2.2, y, t) = \frac{6}{0.41^2} \sin(\pi t/8) y(0.41 - y) \\
 u_2(0, y, t) &= u_2(2.2, y, t) = 0.
 \end{aligned}$$

The viscosity is set as $\nu = 10^{-3}$ and the external force $f = 0$. Here we use our Algorithm 3.1 with $\chi = \Delta t$ with Taylor-Hood element on a triangular mesh with 14,868 DOF, with time step $\Delta t = 0.0005$ and filtering radius δ , chosen to be the average mesh width, with varying indicator functions. The fully resolved computations of the true Navier-Stokes use more than 100,000 DOF and even

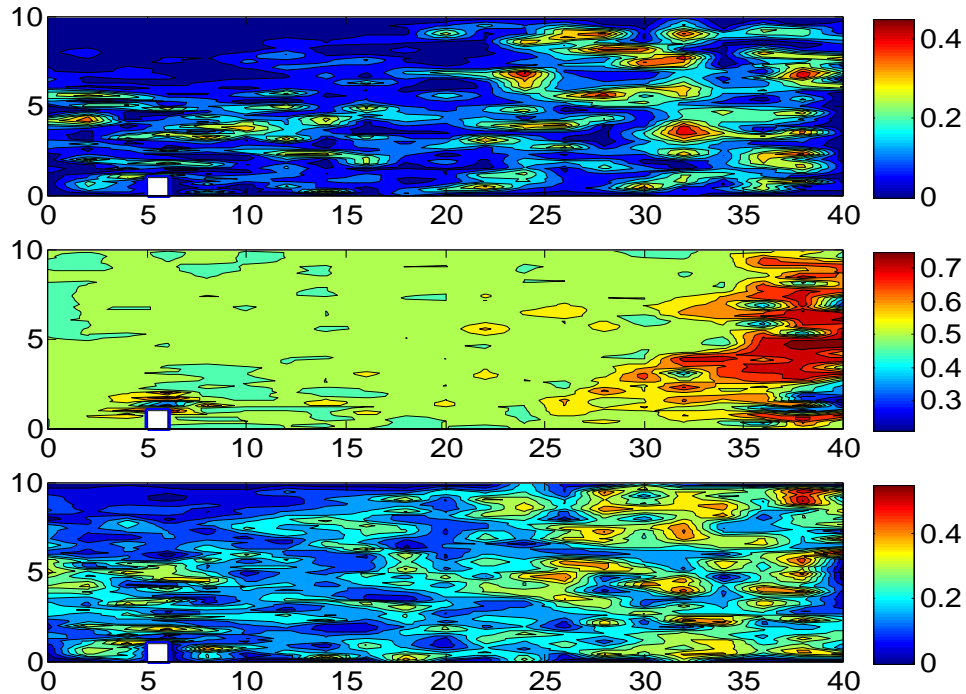


FIGURE 5.3. Contour plots of the Vreman filter, Q-filter and VQ-filter (from top to bottom).

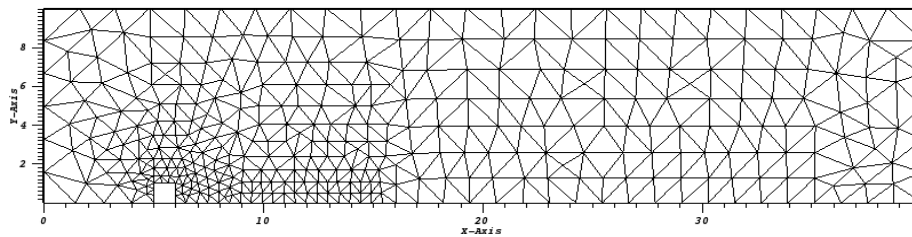


FIGURE 5.4. coarse mesh (1,762 DOF).

smaller time steps. Figure 5.6 is showing the velocity vector and speed contour for Vreman indicator and other indicators gave roughly the same results. We compare the lift and drag reference values computed from our model with the benchmark reference values in Table 5.1. Our reference values match other literatures [7], [33] and [35]. We see that our algorithm performs well overall. Moreover, Vreman filter, Q-filter and VQ indicator filter do give more accurate results than linear filter.

5.3. Comparison between Stokes and Laplace filter. We did a comparison between Stokes filter and Laplace filter with above two 2D problems. Since Vreman and VQ indicator gave better results, here we only included Vreman indicator. For 2D channel flow over a step, we use exactly the same set up for both Stokes and Laplace filter as shown in the first example. The velocity and indicator contour for Laplace filter are shown in Figure 5.7. Here we can see that comparing to Figure 5.6 produced by Stokes filter with Vreman indicator, we get the same answer with

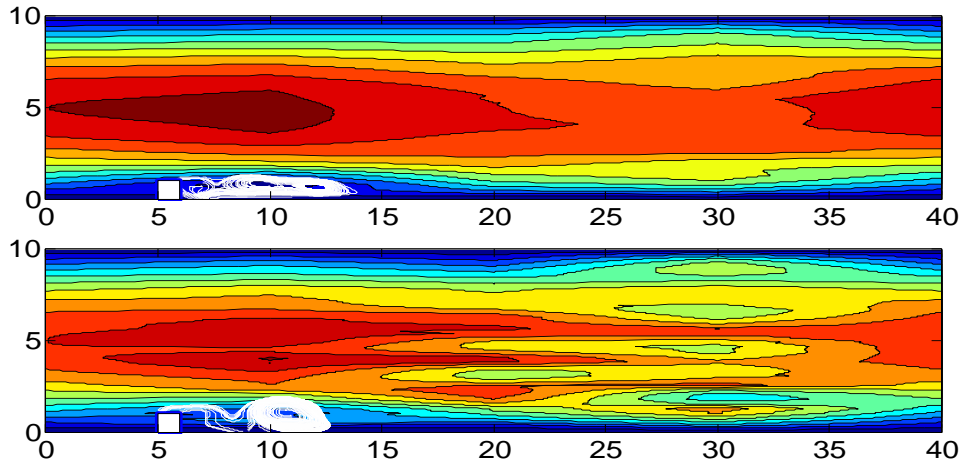


FIGURE 5.5. Velocity solutions for $T = 40$ for 2D flow over a step for the Time Relaxation model with $\chi = 0.1$ using VQ indicator under mesh 1762 DOF(top) (see Figure 5.4) and without Time Relaxation model under the same mesh(bottom).

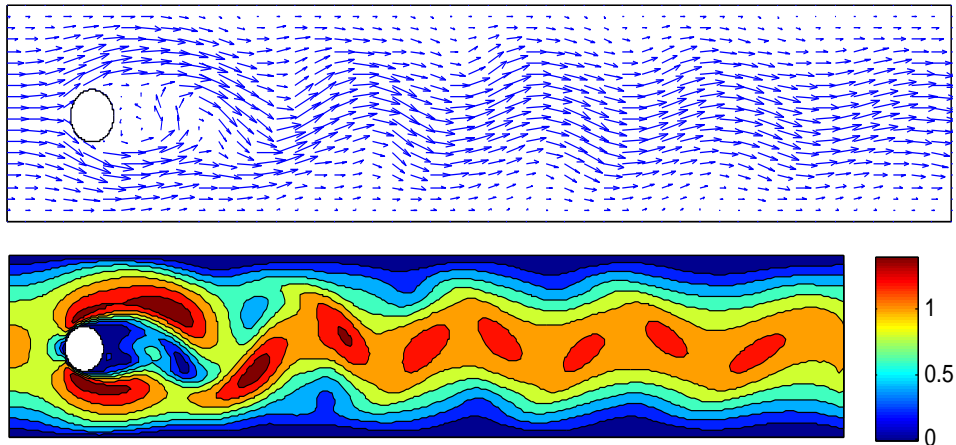


FIGURE 5.6. Velocity field (top) and speed contour (bottom) for $t = 6$ for 2D flow around a cylinder for the Time Relaxation model with $\chi = 0.00125$ using Vreman indicator.

TABLE 5.1. Lift, drag, and pressure drop for the flow around a cylinder experiment with varying indicator functions used in the filtering.

Indicator	DOF	c_d, max	c_l, max	ΔP
$a(u) = 1$	14, 868	2.89928	0.465398	-0.102496
$a_V(u)$	14, 868	2.89931	0.470893	-0.109909
$a_Q(u)$	14, 868	2.89986	0.471104	-0.109956
$a_{VQ}(u)$	14, 868	2.89934	0.471074	-0.109948
John and Rang	2, 347, 776	2.950918381	0.47787543	0.11161567
DNS reference values	> 100, 000	[2.93, 2.97]	[0.47, 0.49]	[-0.115, -0.105]

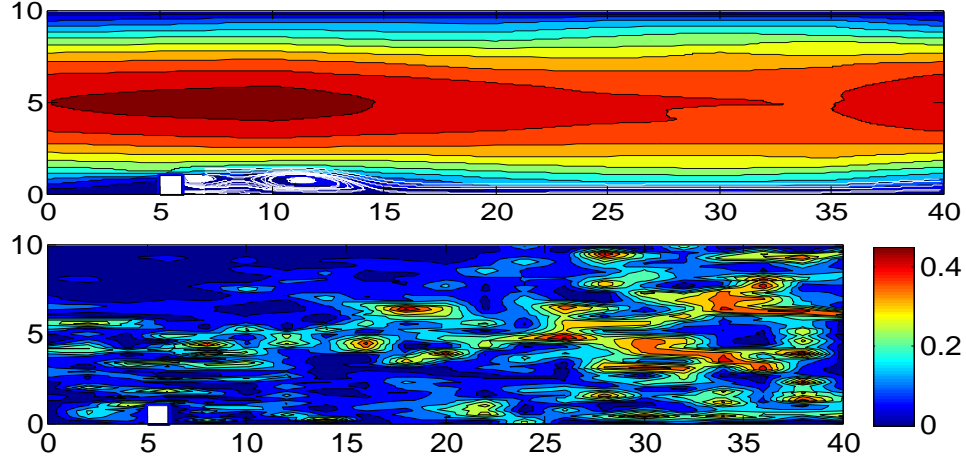


FIGURE 5.7. Velocity contour (top) and Vreman indicator contour (bottom) with Laplace filter for the Time Relaxation model with $\chi = 0.1$.

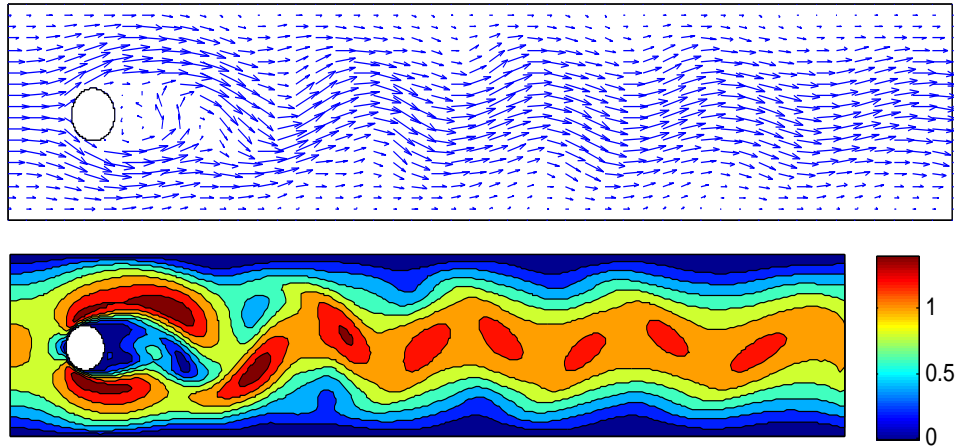


FIGURE 5.8. Velocity field (top) and speed contour (bottom) for $t = 6$ for 2D flow around a cylinder for the Time Relaxation model with $\chi = 0.00125$ using Vreman indicator.

Laplace filter and Vreman indicator. For the 2D flow around a cylinder, with the same set up as Stokes filter in the second example, the Laplace also tend to give the same results. The velocity field and speed contour are given in Figure 5.8. The lift and drag value computed from Laplace filter with Vreman indicator is

$$c_{d, max} = 2.89931, c_{l, max} = 0.471143 \text{ and } \Delta p = -0.109966$$

which are close to the value given by Stokes filter with Vreman indicator in Table 5.1.

5.4. Three dimensional Taylor-Green vortex flow. Our last simulation is three-dimensional Taylor-Green vortex flow from [34]. The Taylor-Green vortex flow is the three-dimensional, incompressible flow that evolves from an initially

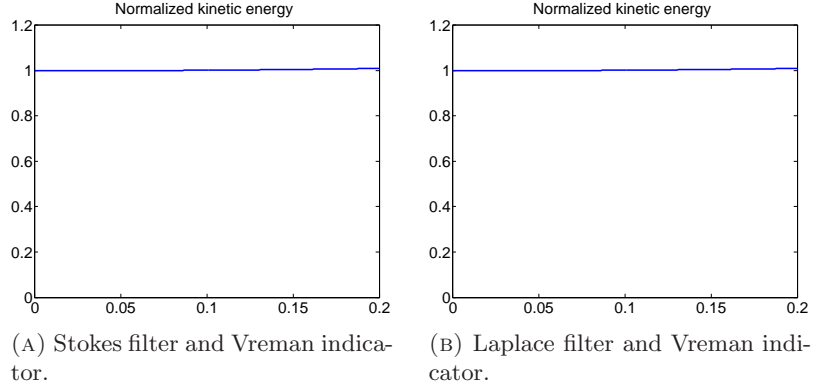


FIGURE 5.9. Normalized kinetic energy for $\nu = 1/1000$ by Time Relaxation model with $\chi = 0.001$ using Stokes filter and Laplace filter with Vreman indicator

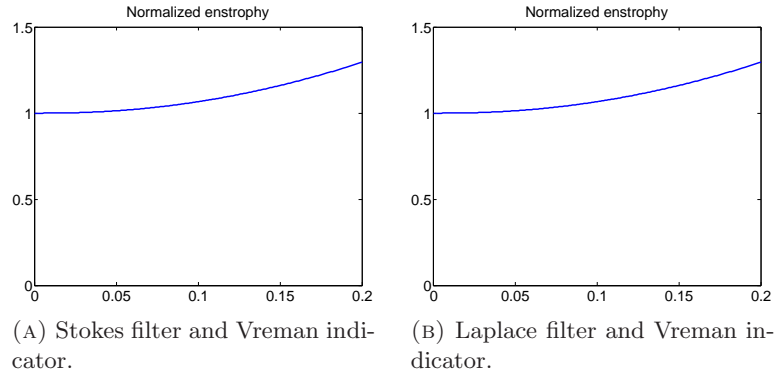


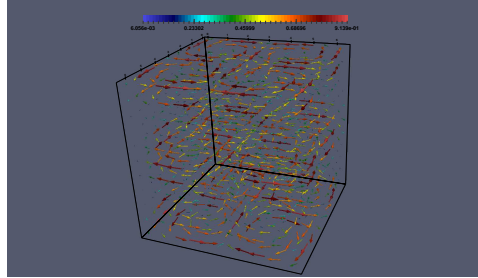
FIGURE 5.10. Normalized enstrophy of Algorithm 3.1 for $\nu = 1/1000$ by Time Relaxation model with $\chi = 0.001$ using Stokes filter and Laplace filter with Vreman indicator

two-dimensional velocity field given by

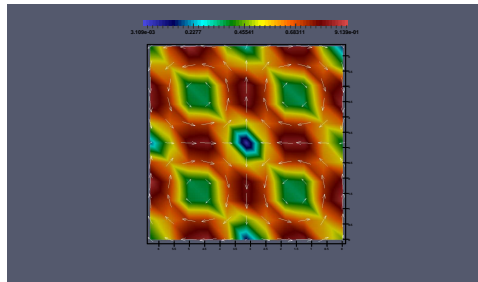
$$(u_1, u_2, u_3)(0) = (\sin(x)\cos(y)\cos(z), -\cos(x)\sin(y)\cos(z), 0),$$

with periodic boundary conditions on $[0, 2\pi]^3$. The initial kinetic energy is $K(0) = \frac{1}{2}\|u(0)\|^2 = \pi^3$, which should be conserved in Taylor-Green Vortex. To show this, we plot the normalized kinetic energy $K(t)/K(0)$. We divided the entire domain into 10 subintervals in all three directions, giving 6000 elements. In the Taylor-Green vortex flow, we expect a growth of enstrophy (defined as $\frac{\nu}{2}\|\nabla u\|^2$)

to be shown by simulation results. We used the time step $\Delta t = 0.001$ and 200 time steps were performed for the viscosity $\nu = 1/1000$. Here, we compare those two filters Stokes filter and Laplace filter both with Vreman indicators. Figures 5.9 and 5.10 show the normalized energy and normalized enstrophy for Stokes filter with Vreman indicator and Laplace filter with Vreman indicator, respectively. From Figures 5.9 and 5.10, we can see that there is not a big difference between using Stokes filter and Laplace filter. We also show the 3D velocity field by Laplace filter and Vreman indicator in 5.11.



(A) 3D velocity field.



(B) 3D velocity field from the view at the top of the domain.

FIGURE 5.11. 3D velocity field by Algorithm 3.1 for $\nu = 1/1000$ by Time Relaxation model with $\chi = 0.001$ using Laplace filter with Vreman indicator

6. Conclusions

In this article, we developed, analyzed and numerically tested a finite element scheme for the family of time relaxation regularization of NSE given by (1)-(2). We have extended and improved the work from [10] by incorporating a nonlinear filtering model. The numerical solutions of the proposed scheme are unconditionally stable, and converge to the true NSE solutions as $\Delta t, h \rightarrow 0$. The numerical experiments show the effectiveness of the nonlinear filter over the linear case. We determined that Vreman and VQ indicator functions perform the best. Also, our time relaxation model gives comparable results with the simpler Laplace filter instead of Stokes filter.

References

- [1] N.A. Adams and S. Stolz, Deconvolution methods for subgrid-scale approximation in large eddy simulation, in *Modern Simulation Strategies for Turbulent Flow*, R.T. Edwards, 2001.
- [2] N.A. Adams and S. Stolz, A subgrid-scale deconvolution approach for shock capturing, *Journal of Computational Physics*, 178, 391–426, (2002).
- [3] G. Baker, Galerkin approximations for the Navier-Stokes equations, Harvard University, Technical Report, 1976.
- [4] L.C. Berselli, T. Iliescu and W. Layton, *Mathematics of Large Eddy Simulation of Turbulent Flows*, Scientific Computation, Springer, Berlin, 2006.
- [5] M. Olshanskii and X. Xiong, A connection between filter stabilization and eddy viscosity models, *Numerical Methods for Partial Differential Equations*, 29(6), 20612080 (2013).
- [6] A. Bowers and L. Rebholz, Increasing accuracy and efficiency in FE computations of the Leray-deconvolution model, *Numerical Methods for Partial Differential Equations*, 28, 720-736, (2012).

- [7] A. Bowers, L. Rebholz, C. Trenchea and A. Takhirov, Improved Accuracy in Regularization Models of Incompressible Flow via Adaptive Nonlinear Filtering, *International Journal for Numerical Methods in Fluids*, 70, 805-828, (2012).
- [8] S.C. Brenner and L.R. Scott, *The Mathematical Theory of Finite Element Methods*, Springer-Verlag, 1994.
- [9] A. Lozovskiy and A. Takhirov, Computationally efficient modular nonlinear filter stabilization for high Reynolds number flows, submitted to *Advances in Computational Mathematics*.
- [10] V. Ervin, W. Layton and M. Neda, Numerical analysis of a higher order time relaxation model of fluids, *International Journal of Numerical Analysis and Modeling*, 4, 648-670, (2007).
- [11] R. Guenanff, Non-stationary coupling of Navier-Stokes/Euler for the generation and radiation of aerodynamic noises, PhD thesis: Dept. of Mathematics, Universite Rennes 1, Rennes, France, 2004.
- [12] M.D. Gunzburger, *Finite Element Methods for Viscous Incompressible Flows* Academic Press, Boston, 1989.
- [13] F. Hecht, New developments in FreeFem++, *J. Numer. Math.*, 20 (3-4), 251-265, (2012).
- [14] J.G. Heywood and R. Rannacher, Finite element approximation of the nonstationary Navier-Stokes problem., Part IV: Error analysis for the second order time discretization, *SIAM Journal on Numerical Analysis*, 2, 353-384, (1990).
- [15] V. John, *Large Eddy Simulation of Turbulent Incompressible Flows*, Springer, Berlin, 2004.
- [16] A.V. Kolmogorov, The local structure of turbulence in incompressible viscous fluids for very large Reynolds number, *Doklady Akademii Nauk SSSR*, 30, 9-13, (1941).
- [17] A. Labovsky, W. Layton, C. Manica, M. Neda and L. Rebholz, The stabilized, extrapolated trapezoidal finite element method for the Navier-Stokes equations, *Computer Methods in Applied Mechanics and Engineering*, 198, 958-974, (2009).
- [18] W. Layton, *Introduction to Finite Element Methods for Incompressible, Viscous Flows*, SIAM publications, 2008.
- [19] W. Layton, C. Manica, M. Neda and L. Rebholz, Numerical Analysis of a high accuracy Leray-deconvolution model of turbulence, *Numerical Methods for Partial Differential Equations*, 24, 555-582, (2008).
- [20] W. J. Layton, C. C. Manica, M. Neda and L. G. Rebholz, Helicity and energy conservation and dissipation in approximate deconvolution LES models of turbulence , *Advances and Applications in Fluid Mechanics*, 4, 1-46, (2008).
- [21] W. J. Layton, L. G. Rebholz and C. Trenchea, Modular Nonlinear Filter Stabilization of Methods for Higher Reynolds Numbers Flow, *Journal of Mathematical Fluid Mechanics*, 14, 325-354, (2012).
- [22] W. Layton and M. Neda, Truncation of scales by time relaxation, *Journal of Mathematical Analysis and Applications*, 325, 788-807, (2007).
- [23] C. Manica, M. Neda, M. Olshanskii and L. Rebholz, Enabling accuracy of Navier-Stokes-alpha through deconvolution and enhanced stability, *Mathematical Modelling and Numerical Analysis*, 45, 277-308, (2011).
- [24] M. Neda, X. Sun and L. Yu, Increasing accuracy and efficiency for regularized Navier-Stokes equations, *Acta Applicandae Mathematicae*, 118, 57-79, (2012).
- [25] Ph. Rosenau, Extending hydrodynamics via the regularization of the Chapman-Enskog expansion, *Physics Review A* 40, 7193, (1989).
- [26] P. Sagaut, *Large Eddy Simulation for Incompressible Flows*, Springer, Berlin, 2001.
- [27] S. Schochet and E. Tadmor, The regularized Chapman-Enskog expansion for scalar conservation laws, *Archive for Rational Mechanics and Analysis*, 119, 95, (1992).
- [28] S. Stolz and N.A. Adams, An approximate deconvolution procedure for large-eddy simulation, *Physics of Fluids*, 11 1699-1701, (1999).
- [29] S. Stolz, N. Adams and L. Kleiser, The approximate deconvolution model for large-eddy simulations of compressible flows and its application to shock-turbulent-boundary-layer interaction, *Physics of Fluids*, 13, 2985-3001, (2001).
- [30] S. Stolz, N. Adams and L. Kleiser, An approximate deconvolution model for large-eddy simulation with application to incompressible wall-bounded flows, *Physics of Fluids*, 13, 997-1015, (2001).
- [31] A.W. Vreman, An eddy-viscosity subgrid-scale model for turbulent shear flow: algebraic theory and applications, *Physics of Fluids*, 6, 3670-3681, (2004).

- [32] A.A. Wray, J.C. Hunt and P. Moin, Eddies stream and convergence zones in turbulent flows, CTR report, CTR-S88, (1988).
- [33] V. John, Reference values for drag and lift of a two-dimensional time-dependent flow around the cylinder, *Int. J. Numer. Methods Fluids*, 44, 777-788, (2004).
- [34] V. Ervin, W. Layton and M. Neda, Numerical Analysis of Filter-Based Stabilization for Evolution Equations, *SIAM Journal on Numerical Analysis*, 50, 2307-2335, 2012
- [35] V. John and J. Rang, Adaptive time step control for the incompressible Navier-Stokes equations, *Comput. Methods Appl. Mech. Engrg.*, 199, 514-524, (2010).

Department of Mathematics, Texas A&M University, College Station, TX 77843, USA.
E-mail: `aziz.takhirov@math.tamu.edu`

Department of Mathematical Sciences, University of Nevada Las Vegas, Las Vegas, NV, 89154-4020, USA.

E-mail: `monika.neda@unlv.edu`

Los Alamos National Laboratory, T-3 Solid Mechanics and Fluid Dynamics, Los Alamos, New Mexico, USA.

E-mail: `jwaters@lanl.gov`